# Ultra-Fast Photovoltaic-Type Deep-Ultraviolet Photodetector using Hybrid Zero-/Two-dimensional Heterojunctions

*Hao Kan,*[†,‡] *Wei Zheng,*[*,§] *Richeng Lin,*[§] *Min Li,*[†,‡] *Chen Fu,*[†] *Huibin Sun,*[†] *Mei Dong,*[§] *Cunhua Xu,*[§] *Jingting Luo,*[*,†] *YongQing Fu,*[⊥] *Feng Huang,*[§]

[†] *Shenzhen Key Laboratory of Advanced Thin Films and Applications, College of Physics and Energy, Shenzhen University, 518060, Shenzhen, China*

[‡] *Key Laboratory of Optoelectronic Devices and Systems of Ministry of Education and Guangdong Province, College of Optoelectronic Engineering, Shenzhen University, 518060, Shenzhen, China*

[§] *State Key Laboratory of Optoelectronic Materials and Technologies, School of Materials, Sun Yat-sen University, Guangzhou 510275, China*

[⊥] *Faculty of Engineering and Environment, Northumbria University, Newcastle upon Tyne, NE1 8ST, UK*

**ABSTRACT:** Deep ultraviolet (DUV) photodetectors have wide-range applications in satellite communications, air purification and missile-plume detection. However, the critical barriers for the currently available wide-bandgap semiconductors films based DUV photodetectors are their low efficiency, complicated processes, and lattice mismatch with substrate. Quantum dots (QDs) devices prepared using solution based methods can solve these problems. However, so far, there are no any reports on

photovoltaic-type DUV photodetector using QDs. In this study, we propose a novel methodology to construct a hybrid Zero-/Two-dimensional DUV photodetector (p-type graphene/ZnS QDs/4H-SiC) with photovoltaic characteristics. The device exhibits excellent selectivity for DUV light and has an ultra-fast response speed (rise time: 28 μs and decay time: 0.75 ms), which are much better than those reported for conventional photoconductive photodetectors.

**KEYWORDS:** deep ultraviolet, ZnS quantum dots, graphene, photovoltaic detector, ultra-fast

## Introduction

Owing to strong absorption by ozone and the atmosphere, deep ultraviolet (DUV) light (200-280 nm) in sunlight is difficult to reach the surface of earth. Therefore, DUV photodetectors are mainly used in satellite, missile-plume detection, and secure communications.[1-5] So far, the sensitive layer materials for the conventional DUV photodetectors are the wide bandgap semiconductor films, such as AlGaN,[6] $Ga_2O_3$,[7-11] and MgZnO.[12] Unfortunately, the preparation processes for these films are often complicated and expensive, and the lattice mismatch between film and the substrate is often a concern for its application.

To solve these problems, solution-processable semiconductor QDs could be used as the sensing layers for the DUV detection. They have the advantages of low cost, high absorption efficiency, tunable bandgaps and compatibility with multiple substrates (including those flexible ones). Due to these, they have already been applied for photodetector.[13-15] In recent years, QDs photodetectors based on ZnO,[16, 17] perovskite,[18, 19] and PbS[20, 21] has been extensively studied and these reported photodetectors have extremely high responsivity and switching ratios, demonstrating their great potentials for the photodetector applications. Unfortunately, due to the relatively narrow band-gaps of these materials, these QDs-based photodetectors commonly work at the wavelengths between long-range ultraviolet (300-400 nm) and NIR (near infrared) regions. Only a few DUV photodetectors based on QDs have been reported.[22, 23] Therefore, there is an urgent need to search for new types of semiconductor QD materials which are sensitive to the DUV.

The Bohr exciton radius of ZnS QDs is ~2.5 nm, which is much smaller than the above mention semiconductors. Based on the quantum confinement effect, the bandgap of ZnS QDs can be further increased by reducing their crystal sizes, which make them much more sensitive to the DUV.[24, 25] At the same time, they have higher exciton binding energy values (~40 meV) and better thermal stability.[26] Therefore, ZnS QDs could be an excellent DUV sensitive material and can be used in the DUV photodetectors.

In this study, we designed and fabricated a DUV photodetector using the ZnS QDs with a PIN structure (p-type graphene/ZnS QDs/4H-SiC). Measurement results showed that the device exhibits extremely high spectral selectivity in the DUV region. The open circuit voltage is approximately 1.1 V at 780 μW/cm$^2$. Under 0V bias, the device has a responsivity of 0.29 mA/W and an EQE of 1.36%. Under pulsed light, the rise and decay time of the device are 28 μs and 0.75 ms respectively, which can meet the needs of practical applications. We believe that this design methodology not only provides a promising solution for the application of QDs in the field of DUV photodetector, but also opens up a new application strategy for application of composites of zero-dimensional (0D) and two-dimensional (2D) nanomaterials.

**Results and Discussions**

Schematic illustration of synthesis procedure of ZnS QDs is shown in Figure 1a. High-angle Annular Dark-field Scanning Transmission Electron Microscopy (HAADF-STEM) image of ZnS QDs is shown in Figure 1b and Figure S1b is the distribution of particle sizes. The grain size of the sample is found to be 1.8~2.7 nm.

Figure S1a is another enlarged HAADF-STEM image while Figure S1 c and d are the corresponding energy dispersive X-ray spectroscopy (EDS) mapping images. Figure 1c shows the UV-visible absorption spectrum of ZnS QDs. A strong exciton absorption peak is located at 265 nm and the corresponding bandgap is 4.68 eV. Compared with band gap value of the bulk ZnS (e.g., 3.7 eV), ZnS QDs show a blue shift of the bandgap value due to the quantum confinement effect. Figure 1d shows the X-ray diffraction (XRD) pattern of the synthesized ZnS QDs. All the diffraction peaks are corresponding to the zinc blende structure of ZnS (JCPD No. 05-0566). The average grain size $D$ of the prepared sample can be calculated according to the Debye-Scherrer formula,

$$D = 0.89\,\lambda / \beta\, Cos\theta \qquad (1)$$

where $D$ is the average grain size of the particles, $\lambda$ is the wavelength of the X-ray, $\beta$ is the full width of the half-maximum of the diffraction peak, and $\theta$ is the diffraction angle. The calculated average grain size of the synthesized ZnS QD is about 2.5 nm, which is consistent with HAADF-STEM results. Figures 1e and f show the high-resolution X-ray Photoelectron Spectroscopy (XPS) of Zn 2p and S 2p, respectively. The peaks of 1022.35 and 1044.97 eV are corresponding to the $Zn^{2+}$ of the Zn 2p 3/2 and Zn 2p1/2, respectively.[27] The binding energy of S 2p is at 161.9 eV, suggesting the presence of $S^{2-}$ ion.[28] And the corresponding XPS survey spectrum of ZnS QDs is shown in Figure S2. The results of XPS indicate that no impurities are present in the synthesized ZnS QDs.

The schematic illustration of the preparation process and the image of the DUV photodetector (p-type graphene/ZnS QDs/4H-SiC) are shown in Figure 2a and S3. It

consists of Ti/Au electrode, transferred p-type graphene, ZnS QDs film, single crystal 4H-SiC substrate and hot-melt In. Here, the single-layer p-type graphene (p-Gr), ZnS QDs film and 4H-SiC single crystal substrate are constructed into a PIN junction. Among them, ZnS QDs are also used as a deep ultraviolet sensitive layer due to its ultra-wide bandgap (4.68 eV). The 4H-SiC single crystal substrate is used as n-type layer. Meanwhile, p-Gr is not only served as a DUV transparent electrode to collect photo-generated carriers, but also formed as a PIN structure, together with a sensitive layer and a substrate layer. In order to determine the presence of graphene, the Raman spectra of the p-Gr is shown in Figure 2c. The D, G and 2D bands of graphene are centered at 1343, 1589 and 2860 $cm^{-1}$, respectively. A cross-sectional scanning electron microscope (SEM) image shown in Figure 2b confirms that the effective thickness of the ZnS QDs film was about 315 nm. The surface morphology image of the ZnS QDs film with different magnifications are shown in Figures S4 a and b. It can be seen that there are micro-cracks on the surface of the ZnS QDs film, which is caused by the substitution of long oleylamines ligands by short inorganic ligands during the process of ligand exchange.[29] The I-V characteristic curve of the device in dark is shown in Figure 2d. The device exhibits an excellent rectification characteristic, which is attributed to the PIN-type photodiode formed by the p-type graphene, ZnS QDs film and 4H-SiC substrate. In dark state, the forward current of the device is 55.64 nA at 3V, and the rectifying ratio is 43 compared with reverse current at -3V. The absorption spectrum of the as-synthesized ZnS QDs，those aged for 5 days in air and ZnS QDs film after ligand exchange were shown in Figure S5. The absorption spectrum of the

synthesized ZnS QDs was unchanged after they storage in air for 5 days. This suggests the excellent stability of synthesized ZnS QDs. Compared with the synthesized ZnS QDs, the exciton peaks of ZnS QDs film show a red shift after ligand exchange, which is due to the improved coupling between neighboring QDs and enhanced dielectric constant of the QDs thin film.[30] The current-voltage (I-V) characteristics of the ZnS QDs film/4H-SiC DUV photodetector in dark and under DUV condition are shown in Figure S6. The $I_{photo}/I_{dark}$ is about 1.6 under 250 nm light illumination with 3V bias. It did not show rectification characteristics compared to p-Gr/ZnS QDs film/4H-SiC heterostructures.

In order to study the performance of this PIN device based on the ZnS QDs, a series of DUV tests were performed. Figure 3a shows the I-V characteristics of the device under the irradiation of 250 nm DUV light (red spheres) and that under dark state (black spheres). The device exhibits an open circuit voltage of approximately 1.1 V, and the electromotive force of p-Gr higher than the 4H-SiC. Figure 3b shows the corresponding time-voltage (T-V) curve. The open circuit voltage of the device maintains a good stability under the DUV light illumination. Figure 3c shows the relationship between the open circuit voltage of the device and the light intensity illuminated by a 250 nm DUV light source. The open circuit voltage is about 0.49 mV when the optical power density is 24 $\mu W/cm^2$. It can be seen that as the optical power increases, the open circuit voltage gradually increases and tends to be saturated. When the optical power is increase to 1.9 $mW/cm^2$, the open circuit voltage of the device reaches to 1.22 V.

To further understand the performance of the DUV detector based on the ZnS QDs, we measured its current switching behavior at 0 V bias. As shown in Figure 3d, the current can effectively switch continuously, when the light source switches periodically. This is indicating that the detector has extremely high response speed and excellent repeatability. This is due to the fact that the device can work based on the photovoltaic effect. In this device, a built-in electric field will form in ZnS QDs film. Under 250 nm LED illumination, photogenerated e-h pairs are generated by ZnS QDs film and quickly separated by the built-in electric field, moving from PIN (p-type graphene/ZnS QDs/4H-SiC) heterojunction to electrode. Therefore, the photocurrent is produced without external bias. The photocurrent of the device is stable at 7 nA with a light intensity of 191 μW/cm$^2$ under a 250 nm LED illumination, while the current drops to 0.17 nA under the dark state (the switching ratio is approximately 44). Figure 3e shows the dependence of photocurrent on the incident light intensity, which is another important characteristic of the device. By switching the 250 nm LED on and off at 5 second intervals under the light illumination in a range of 155 to 184 μW/cm$^2$, the device exhibits a stable periodic response with the switching of the 250 nm LED light at a bias of 0 V, and the photocurrent increases as the incident light intensity increases. Figure 3f shows the quantitative relationship between the photocurrent extracted and the intensity of the incident light obtained from Figure 3e. It is observable that the photocurrent exhibits a power-law dependence on the light intensity with an index of 0.73 ($I_p = P^{0.73}$), and this non-integer index is associated with the trap state of the ZnS QDs film.

The performance of this DUV photodetector can be quantitatively evaluated by calculating the responsivity ($R$) and specific detection rate ($D^*$) of the DUV photodetector, which can be calculated by:[31, 32]

$$R = \frac{I_P - I_D}{P} \quad (2)$$

$$D^* = \frac{(I_P - I_D)\ \sqrt{A}}{P\sqrt{2eI_D}} \quad (3)$$

where $I_P$ is the photocurrent, $I_D$ is the dark current, $P$ is the intensity of light incident on the device, $A$ is the effective area of the sensitive area, and $e$ is the electron charge. From the above two equations, the optical response of the device at 0V bias can be calculated to be 0.29 mA/W, and the obtained specific detection rate is $1.41\times10^{10}$ jones. In addition, the EQE of the device can be calculated by:[33, 34]

$$EQE = \frac{hcR}{e\lambda} \quad (4)$$

where $h$ is Planck constant, $c$ is the velocity of the incident light, $e$ is the charge, and $\lambda$ is the wavelength of the incident light. It can be calculated that the EQE of the device under 155 μW/cm$^2$ light density at a wavelength of 250 nm is 1.36%. The above results, suggest that this DUV photodetector has a high responsivity without external bias.

Temporal-response speed is another important parameter of photodetectors, which demonstrates the ability of the device to respond to high frequency optical signals. Here, we used a 193 nm pulsed laser as the ultra-fast-changing UV light signal and measured the time responses of the photovoltaic device, as shown in Figure 4a. The time-dependent photo-response period signal is shown in Figure 4b, and the device can reproduce the optical pulse signal very well. The rise time ($T_{90}$) is defined as the time

spent by photocurrent approaching 90% of the maximum photocurrent, and the decay time ($T_{10}$) is considered as the time photocurrent needs to get back to 10% of the maximum photocurrent.[16] Then, the rise and decay time of the device can be analyzed by extending the coordinate axis. It can be seen that the rise and decay time of this DUV photodetector are 28 μs and 0.75 ms, respectively (Figure 4c, 4d), which indicate that this device has the ability to follow the rapidly changed optical signals. Table 1 summarizes the reported performance of photodetectors based on different QDs from the literature. Compared with most of the other QDs photodetectors, present photodetector based on ZnS QDs shows extremely fast response speeds. We believe that the ultrafast response speed of such a device is attributed to the built-in electric field in p-Gr/ZnS QDs film/4H-SiC, which allows photogenerated carriers to be rapidly separated.

Figure 5a shows the responsivity spectrum of the device without bias (dark circle). At a wavelength of 250 nm, the responsivity is 0.29 mA/W, indicating that the photodetector can be used to detect the DUV without any external bias. When the incident wavelengths are changed to 280 nm and 310 nm, the responsivity values of the device are only 0.036 mA/W and 0.0068 mA/W, respectively. This is suggesting good selectivity of the photodetector for the DUV. In addition, the device has a DUV-UVA injection ratio [R(250 nm)/R(365 nm)] of $3.89\times10^2$, further demonstrating its excellent selectivity for the DUV.

The energy band diagram of the device is shown in Figure 5b. At 0V bias, a built-in electric field is formed at the interface between the p-Gr and the ZnS QDs film, and

its direction is directed from ZnS QDs film to p-Gr. The exciton peak of the ZnS QDs film is located at 270 nm. Hence, under the illumination of 250 nm UV light, photogenerated electron hole pairs produce in ZnS QDs film. When the 250 nm DUV light is incident on the surface of the ZnS QDs film, the electron-hole pairs generated from the ZnS QDs film are separated by the built-in electric field, where the holes drift towards the graphene surface, whereas the electrons move towards 4H-SiC. For this vertical-structure photovoltaic detector, its carrier transit time is much shorter than the recombination time of the electron and hole. This enables a relatively fast DUV photoresponse time.[35] Under 250 nm UV light illumination, the open circuit voltage of the device is about 1.2 V at 1.9 mW/cm$^2$, forming a photovoltaic based ultraviolet photodetector.

## CONCLUSION

In summary, a PIN DUV photovoltaic-type detector based on ZnS QDs was successfully designed and tested, in which ZnS QDs were deposited on the 4H-SiC substrate using spin coating. It is worth noting that this PIN photodetector based on ZnS QDs exhibited an outstanding spectral selectivity for the DUV. Under 250 nm light illumination of 184 μW/cm$^2$, the responsivity of the device was 0.29 mA/W without external bias. In addition, the device shows an ultrafast rise and decay time (28 μs / 0.75 ms) under 193 nm pulsed laser illumination. This work not only lays a foundation for the application of QDs in the field for DUV detection, but also paves a new way to composite 2D and 0D nanomaterials.

## METHODS

**Synthesis of ZnS Quantum Dots**. The ZnS QDs were synthesized using a modified heat-up method.[36] 4.41g of zinc stearate ($ZnSt_2$), 0.225 g of thioacetamide (TAA), 6 ml of oleylamine(OLA) and 50 mL of octadecene (ODE) were added into a 100 mL volume three-necked flask. The flask was degassed under the vacuum at room temperature and heated to 140 °C for 1 h under nitrogen. After the reaction was completed, the solution was quickly cooled down to room temperature. Further, the precipitate was washed 2-3 times using hexane, and ethanol and then dispersed for use in octane.

**Device preparation.** The single crystals of 4H-SiC were purchase from KMT corporation, China. The film was deposited using a spin-coating method as described below. Briefly, 40 μL of ZnS QD solution was deposited on the surface of 4H-SiC by spin-coating at 3000 rpm for 30 seconds. The obtained ZnS QDs film was then immersed in a hexadecyltrimethylammonium bromide (CTAB) solution (10 mg/mL in anhydrous methanol) for 45 seconds. The CTAB solution was spun at a speed of 3000 rpm for 30 s. Lastly, the film was washed three times with anhydrous methanol. After repeating the above process for three times, a ZnS QDs film with a given thickness was obtained on 4H-SiC. After depositing the ZnS QDs film, the target size graphene was constructed on the surface of the ZnS QDs film using a wet transfer method. Then, 50 nm Ti and 50 nm gold were deposited on the graphene edge using a thermal evaporation method. Finally, we used hot-melt indium (In) as the electrode on the side of the 4H-

SiC.

**Characterization and Measurements.** The X-ray diffraction (XRD) measurement was performed using an X-ray diffractometer (MAXima_XXRD-7000, Shimadzu, Japan). The shape and size of ZnS QDs was characterized using a Titan Cubed Themis G2 300. Morphologies of the ZnS QDs films were obtained using a FEI model SIRION 200 microscope. The absorption spectra of the ZnS QDs were recorded using a UV-vis-NIR spectrophotometer (UV 3600 Plus, Japan). XPS measurements were performed using a Thermo-VG Scienti*fi*c ESCALab 250 microprobe. Photodetector device performance was measured using the SourceMeter Keithley 2636B. Lighting was generated through an Agilent source controlled a 250 nm semiconductor light-emitting diode (LED). The spectral response was measured by LEDs or lasers. In the high-speed photoresponse test shown in Figure 4, an ArF laser with a wavelength of 193 nm was used as a pulse light source, and an oscilloscope (Keysight DSOS604A) was used to acquire a high-speed voltage signal.

## FIGURES

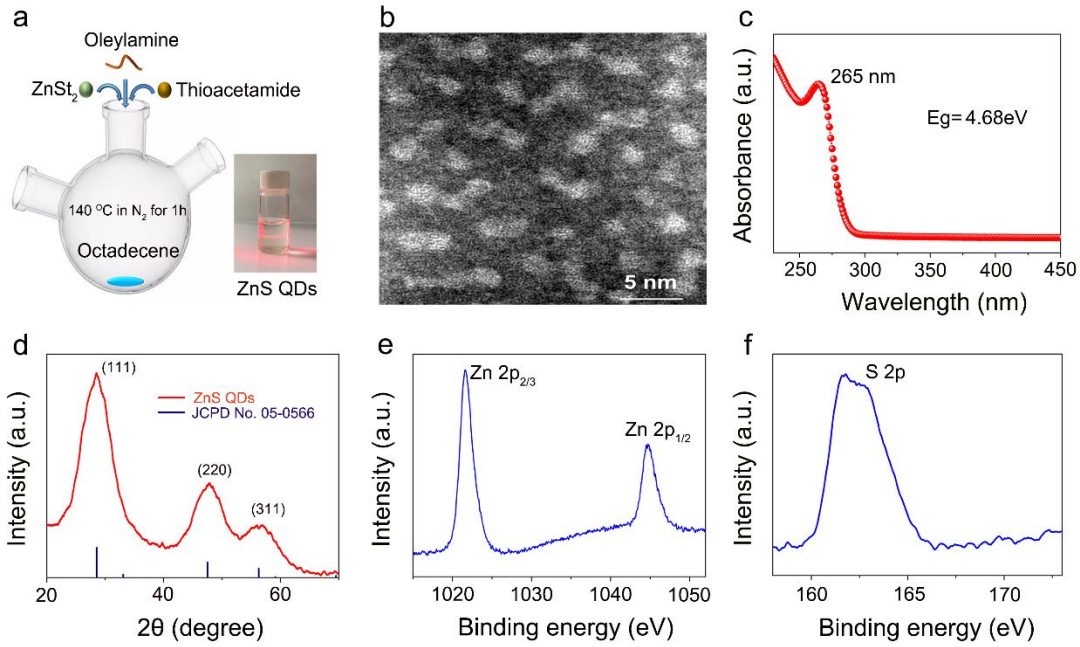


**Figure 1.** (a) Schematic illustration of synthesis procedure of ZnS QDs. (b) HAADF-STEM images of the ZnS QDs. (c)UV–vis absorption spectrum of the ZnS QDs (d) XRD pattern of ZnS QDs. XPS spectra of (e) Zn 2p and (f) S 2p of the ZnS QDs.

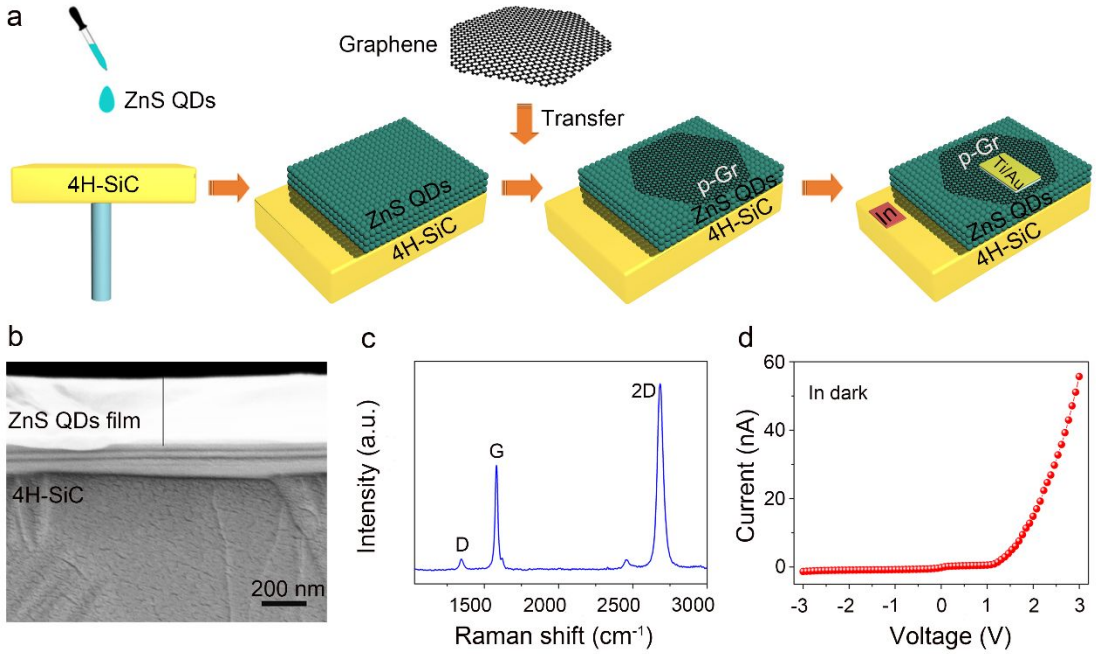


**Figure 2.** (a) Fabrication procedure of the DUV photodetector (p-type graphene/ZnS QDs/4H-SiC). (b) Cross-sectional SEM image of the device. (c) The Raman spectra of the Graphene (d) I–V curves of the device in dark.

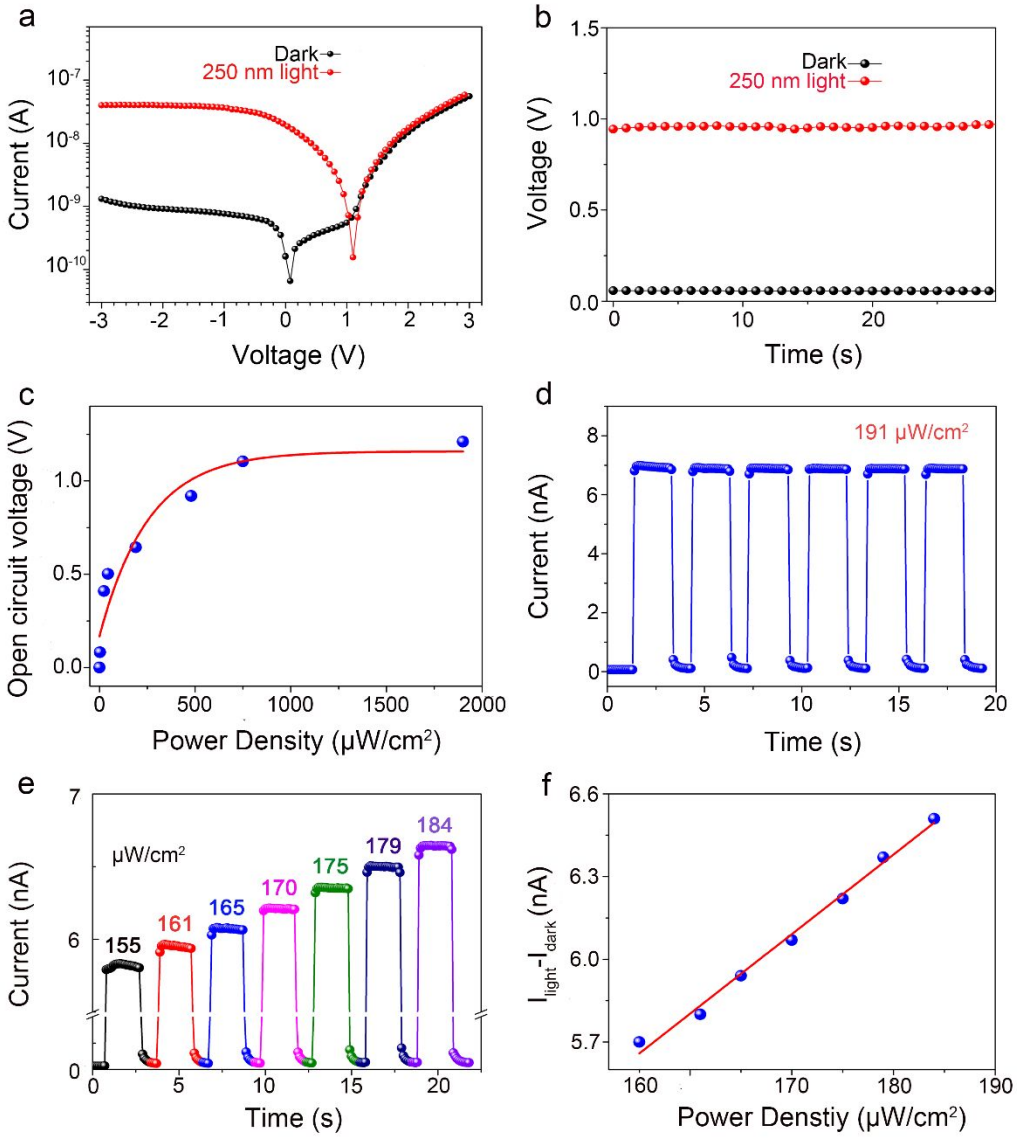


**Figure 3.** DUV photovoltaic testing (a) I−V characteristics of the device under dark conditions and illuminated with 250 nm UV light. (b) Voltage-Time output results of the device under dark and illuminated with 250 nm UV light. (c)The dependence of open circuit voltage on UV light intensity. (d) Time-resolved DUV photoresponse of the device under 250 nm DUV light illumination (191 μW/cm$^2$) without bias. (e) Light intensity dependent photoresponse of the device irradiated by 250 nm LED without bias. (f) The dependence of photocurrent on light intensity without bias.

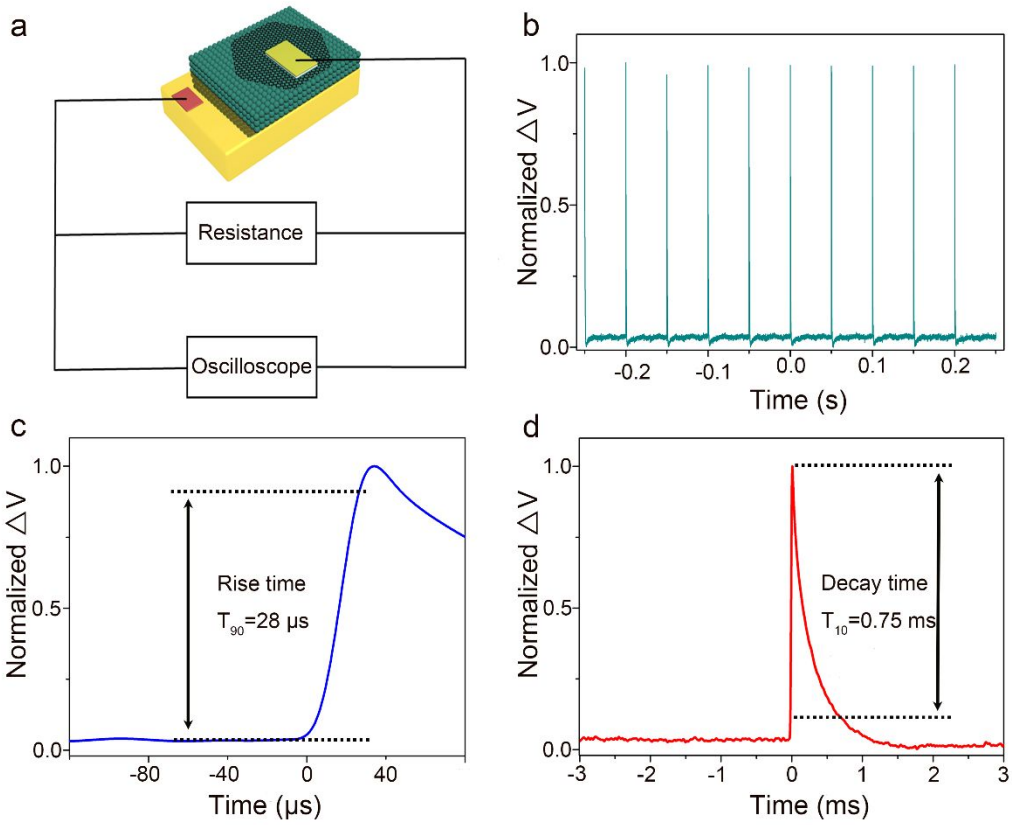


**Figure 4.** (a) Schematic diagram of the photovoltaic response under 193 nm light with a nanosecond pulse. (b) Voltage output signal of the device generated under 10 equal interval pulses. (c) Relationship between rise time (μs) and normalized ΔV. (d). Relationship between decay time (ms) and normalized ΔV.

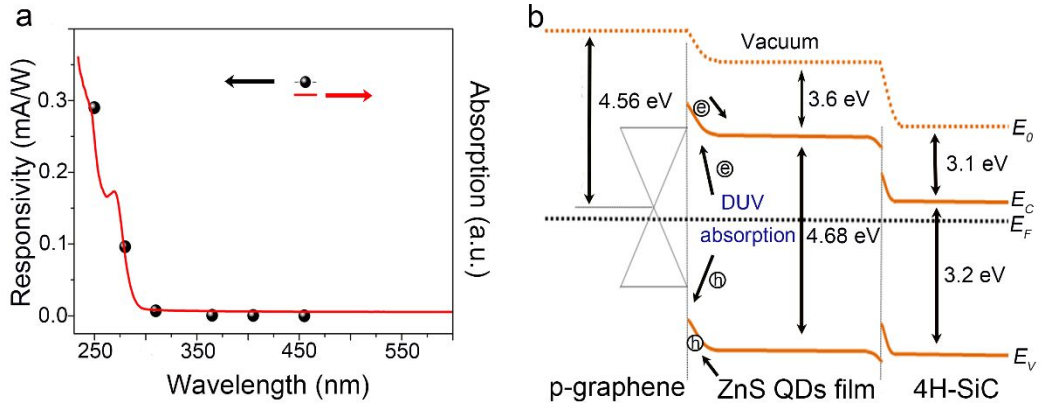


**Figure 5.** (a) Responsivity spectrum of the device at different LED wavelengths (dark circle) and the absorption of the ZnS film (red line). (b) Energy band diagram of p-Gr/ZnS QDs film/ 4H-SiC heterostructure.

**Table 1.** Comparison of the characteristic photoresponse parameters of the photodetector based on QDs

| Materials | Wavelength | Bias | Rise time | Decay time | Ref. |
|---|---|---|---|---|---|
| ZnS QDs | 254 nm | 40 V | 0.35 s | 0.07 s | 22 |
| ZnO QDs | 224.3 nm | 5 V | <0.08 s | <0.08 s | 23 |
| ZnO QDs/G | 330 nm | 10 V | 5 s | 85.1 s | 37 |
| Graphene QDs | 254 nm | 5 V | 0.064 s | 0.023 s | 38 |
| ZnO QDs | 325 nm | 5 V | 0.8 s | 0.5 s | 39 |
| Graphene QDs /ZnO Nanorods | 365 nm | 2 V | 2.14 s | 0.91 s | 40 |
| ZnO QDs/$Zn_2SnO_4$ Nanowire | 300 nm | 0.1 V | 0.047 s | - | 41 |
| p-Gr/ZnS QDs/4H-SiC | 250 nm | 0 V | 0.000028 s | 0.00075 s | This work |

## ASSOCIATED CONTENT

### Supporting information

The Supporting Information is available free of charge on the ACS Publications website at DOI. STEM; XPS spectra; An image of the fabricated DUV photodetector; SEM image of the ZnS QDs film; Absorption spectrum of as-synthetized ZnS QDs, ZnS QDs aged for 5 days in air and ZnS QDs film after ligand exchange; Current-voltage (I-V) characteristics of the ZnS QDs film/4H-SiC DUV photodetector.

## AUTHOR INFORMATION

### Corresponding Author

*Email: zhengw37@mail.sysu.edu.cn (W. Zheng);

*Email: luojt@szu.edu.cn (JT. Luo)

### Notes

The authors declare no competing financial interest

## ACKNOWLEDGMENTS

The authors gratefully acknowledge the support of Research and Development Program of China (Grant no. 2016YFB0402705), National Natural Science Foundation of China (Grant no. 11704261, 11575118, 61604178), Natural Science Foundation of SZU (Grant no. 2017067), Shenzhen Key Lab Fund (ZDSYS20170228105421966), Shenzhen Science & Technology Project (Grant no. JCYJ20170817100658231). Funding supports from UK Engineering Physics and Science Research Council

(EPSRC EP/P018998/1), Newton Mobility Grant (IE161019) through Royal Society and NFSC, and Royal academy of Engineering UK-Research Exchange with China and India are acknowledged. The authors wish to acknowledge the assistance on STEM observation received from the Electron Microscope Center of the Shenzhen University.

## REFERENCE

(1) Zheng, W.; Huang, F.; Zheng, R.; Wu, H., Low-Dimensional Structure Vacuum-Ultraviolet-Sensitive (lambda < 200 nm) Photodetector with Fast-Response Speed Based on High-Quality AlN Micro/Nanowire. *Adv. Mater.* **2015,** *27* (26), 3921-3927.

(2) Zheng, W.; Lin, R.; Ran, J.; Zhang, Z.; Ji, X.; Huang, F., Vacuum-Ultraviolet Photovoltaic Detector. *ACS Nano* **2018,** *12* (1), 425-431.

(3) Zhuo, Y.; Chen, Z.; Tu, W.; Ma, X.; Pei, Y.; Wang, G., β-$Ga_2O_3$ Versus ε-$Ga_2O_3$ : Control of the Crystal Phase Composition of Gallium Oxide Thin Film Prepared by Metal-Organic Chemical Vapor Deposition. *Appl. Surf. Sci.* **2017,** *420*, 802-807.

(4) Zheng, W.; Lin, R.; Zhang, D.; Jia, L.; Ji, X.; Huang, F., Vacuum-Ultraviolet Photovoltaic Detector with Improved Response Speed and Responsivity via Heating Annihilation Trap State Mechanism. Adv. *Optical Mater.* **2018,** *6* (21), 1800697.

(5) Zheng, W.; Lin, R.; Jia, L.; Huang, F., Vacuum Ultraviolet Photovoltaic Arrays. *Photonics Research* **2018,** *7* (1), 98.

(6) Zhang, W.; Xu, J.; Ye, W.; Li, Y.; Qi, Z.; Dai, J.; Wu, Z.; Chen, C.; Yin, J.; Li, J.; Jiang, H.; Fang, Y., High-Performance AlGaN Metal–Semiconductor–Metal Solar-Blind Ultraviolet Photodetectors by Localized Surface Plasmon Enhancement. *Appl.*

*Phys. Lett.* **2015,** *106* (2), 021112.

(7) Dong, M.; Zheng, W.; Xu, C.; Lin, R.; Zhang, D.; Zhang, Z.; Huang, F., Ultrawide-Bandgap Amorphous MgGaO: Nonequilibrium Growth and Vacuum Ultraviolet Application. Adv. *Optical Mater.* **2018**, 1801272.

(8) Lin, R.; Zheng, W.; Zhang, D.; Zhang, Z.; Liao, Q.; Yang, L.; Huang, F., High-Performance Graphene/beta-$Ga_2O_3$ Heterojunction Deep-Ultraviolet Photodetector with Hot-Electron Excited Carrier Multiplication. *ACS Appl. Mater. Interfaces* **2018,** *10* (26), 22419-22426.

(9) Chen, Z.; Li, Z.; Zhuo, Y.; Chen, W.; Ma, X.; Pei, Y.; Wang, G., Layer-by-Layer Growth of ε-$Ga_2O_3$ Thin Film by Metal–Organic Chemical Vapor Deposition. *Applied Physics Express* **2018,** *11* (10), 101101.

(10) Zhang, D.; Zheng, W.; Lin, R. C.; Li, T. T.; Zhang, Z. J.; Huang, F., High Quality β-$Ga_2O_3$ Film Grown with N2O for High Sensitivity Solar-Blind-Ultraviolet Photodetector with Fast Response Speed. *J. Alloys Compd.* **2018,** *735*, 150-154.

(11) Xu, C.; Du, Z.; Huang, Y.; Dong, M.; Lin, R.; Li, Y.; Wang, B.; Zheng, W.; Huang, F., Amorphous-MgGaO Film Combined with Graphene for Vacuum-Ultraviolet Photovoltaic Detector. *ACS Appl. Mater. Interfaces* **2018,** *10*, 42681-42687.

(12) Kaneko, K.; Tsumura, K.; Ishii, K.; Onuma, T.; Honda, T.; Fujita, S., Deep-Ultraviolet Luminescence of Rocksalt-Structured $Mg_xZn_{1-x}O$ ($x > 0.5$) Films on MgO Substrates. *J. Electron. Mater.* **2018,** *47* (8), 4356-4360.

(13) Clifford, J. P.; Konstantatos, G.; Johnston, K. W.; Hoogland, S.; Levina, L.; Sargent, E. H., Fast, Sensitive and Spectrally Tuneable Colloidal-Quantum-Dot

Photodetectors. *Nat Nanotechnol* **2009,** *4* (1), 40-44.

(14) Konstantatos, G.; Howard, I.; Fischer, A.; Hoogland, S.; Clifford, J.; Klem, E.; Levina, L.; Sargent, E. H., Ultrasensitive Solution-Cast Quantum Dot Photodetectors. *Nature* **2006,** *442* (7099), 180-183.

(15) Nian, Q.; Gao, L.; Hu, Y.; Deng, B.; Tang, J.; Cheng, G. J., Graphene/PbS-Quantum Dots/Graphene Sandwich Structures Enabled by Laser Shock Imprinting for High Performance Photodetectors. *ACS Appl. Mater. Interfaces* **2017,** *9* (51), 44715-44723.

(16) Liu, S.; Li, M. Y.; Su, D.; Yu, M.; Kan, H.; Liu, H.; Wang, X.; Jiang, S., Broad-Band High-Sensitivity ZnO Colloidal Quantum Dots/Self-Assembled Au Nanoantennas Heterostructures Photodetectors. *ACS Appl. Mater. Interfaces* **2018,** *10* (38), 32516-32525.

(17) Guo, W.; Xu, S.; Wu, Z.; Wang, N.; Loy, M. M.; Du, S., Oxygen-Assisted Charge Transfer Between ZnO Quantum Dots and Graphene. *Small* **2013,** *9* (18), 3031-3036.

(18) Yang, Z.; Wang, M.; Li, J.; Dou, J.; Qiu, H.; Shao, J., Spray-Coated $CsPbBr_3$ Quantum Dot Films for Perovskite Photodiodes. *ACS Appl. Mater. Interfaces* **2018,** *10* (31), 26387-26395.

(19) Wu, H.; Kang, Z.; Zhang, Z.; Zhang, Z.; Si, H.; Liao, Q.; Zhang, S.; Wu, J.; Zhang, X.; Zhang, Y., Interfacial Charge Behavior Modulation in Perovskite Quantum Dot-Monolayer $MoS_2$ 0D-2D Mixed-Dimensional van der Waals Heterostructures. *Adv. Funct. Mater.* **2018,** *28* (34), 1802015.

(20) Ren, Z.; Sun, J.; Li, H.; Mao, P.; Wei, Y.; Zhong, X.; Hu, J.; Yang, S.; Wang, J., Bilayer PbS Quantum Dots for High-Performance Photodetectors. *Adv. Mater.* **2017,** *29* 1702055.

(21) He, J.; Qiao, K.; Gao, L.; Song, H.; Hu, L.; Jiang, S.; Zhong, J.; Tang, J., Synergetic Effect of Silver Nanocrystals Applied in PbS Colloidal Quantum Dots for High-Performance Infrared Photodetectors. *ACS Photonics* **2014,** *1* (10), 936-943.

(22) Xia, Y.; Zhai, G.; Zheng, Z.; Lian, L.; Liu, H.; Zhang, D.; Gao, J.; Zhai, T.; Zhang, J., Solution-Processed Solar-Blind Deep Ultraviolet Photodetectors Based on Strongly Quantum Confined ZnS Quantum Dots. *J. Mater. Chem. C* **2018,** *6* (42), 11266-11271.

(23) Mitra, S.; Aravindh, A.; Das, G.; Pak, Y.; Ajia, I.; Loganathan, K.; Di Fabrizio, E.; Roqan, I. S., High-Performance Solar-Blind Flexible Deep-UV Photodetectors Based on Quantum Dots Synthesized by Femtosecond-Laser Ablation. *Nano Energy* **2018,** *48*, 551-559.

(24) Deng, Z.; Tong, L.; Flores, M.; Lin, S.; Cheng, J. X.; Yan, H.; Liu, Y., High-Quality Manganese-Doped Zinc Sulfide Quantum Rods with Tunable Dual-Color and Multiphoton Emissions. *J. Am. Chem. Soc.* **2011,** *133* (14), 5389-5396.

(25) Zhu, G.; Zhang, S.; Xu, Z.; Ma, J.; Shen, X., Ultrathin ZnS Single Crystal Nanowires: Controlled Synthesis and Room-Temperature Ferromagnetism Properties. *J. Am. Chem. Soc.* **2011,** *133* (39), 15605-15612.

(26) Kuang, W.; Liu, X.; Li, Q.; Liu, Y.; Su, J.; Tolner, H., Solution-Processed Solar-Blind Ultraviolet Photodetectors Based on ZnS Quantum Dots. *IEEE Photonic Tech.*

*L.* **2018,** *30* (15), 1384-1387.

(27) Poornaprakash, B.; Ramu, S.; Park, S.-H.; Vijayalakshmi, R. P.; Reddy, B. K., Room Temperature Ferromagnetism in Nd Doped ZnS Diluted Magnetic Semiconductor Nanoparticles. *Mater. Lett.* **2016,** *164*, 104-107.

(28) Ramu, S.; Vijayalakshmi, R. P., Effect of Terbium Doping on the Structural and Magnetic Properties of ZnS Nanoparticles. *J. Supercond. Nov. Magn.* **2017,** *30* (7), 1921-1925.

(29) Klem, E. J. D.; Shukla, H.; Hinds, S.; MacNeil, D. D.; Levina, L.; Sargent, E. H., Impact of Dithiol Treatment and Air Annealing on the Conductivity, Mobility, and Hole Density in PbS Colloidal Quantum Dot Solids. *Appl. Phys. Lett.* **2008,** *92* (21), 212105.

(30) Zarghami, M. H.; Liu, Y.; Gibbs, M.; Gebremichael, E.; Webster, C.; Law, M., p-Type PbSe and PbS Quantum Dot Solids Prepared with Short-Chain Acids and Diacids. *ACS Nano* **2010,** *4* (4), 2475-2485.

(31) Zheng, W.; Lin, R.; Zhang, Z.; Huang, F., Vacuum-Ultraviolet Photodetection in Few-Layered h-BN. *ACS Appl. Mater. Interfaces* **2018,** *10* (32), 27116-27123.

(32) Zheng, W.; Zhang, Z.; Lin, R.; Xu, K.; He, J.; Huang, F., High-Crystalline 2D Layered $PbI_2$ with Ultrasmooth Surface: Liquid-Phase Synthesis and Application of High-Speed Photon Detection. *Adv. Electron. Mater.* **2016,** *2* (11), 1600291.

(33) Zheng, W.; Xiong, X.; Lin, R.; Zhang, Z.; Xu, C.; Huang, F., Balanced Photodetection in One-Step Liquid-Phase-Synthesized $CsPbBr_3$ Micro-/Nanoflake Single Crystals. *ACS Appl. Mater. Interfaces* **2018,** *10* (2), 1865-1870.

(34) Zheng, W.; Lin, R.; Zhang, Z.; Liao, Q.; Liu, J.; Huang, F., An Ultrafast-Temporally-Responsive Flexible Photodetector with High Sensitivity Based on High-Crystallinity Organic-Inorganic Perovskite Nanoflake. *Nanoscale* **2017,** *9* (34), 12718-12726.

(35) Guo, F.; Yang, B.; Yuan, Y.; Xiao, Z.; Dong, Q.; Bi, Y.; Huang, J., A Nanocomposite Ultraviolet Photodetector Based on Interfacial Trap-Controlled Charge Injection. *Nat Nanotechnol* **2012,** *7* (12), 798-802.

(36) Jia, G.; Banin, U., A General Strategy for Synthesizing Colloidal Semiconductor Zinc Chalcogenide Quantum Rods. *J. Am. Chem. Soc.* **2014,** *136* (31), 11121-11127.

(37) Gong, M.; Liu, Q.; Cook, B.; Kattel, B.; Wang, T.; Chan, W.-L.; Ewing, D.; Casper, M.; Stramel, A.; Wu, J. Z., All-Printable ZnO Quantum Dots/Graphene van der Waals Heterostructures for Ultrasensitive Detection of Ultraviolet Light. *ACS Nano* **2017,** *11* (4), 4114-4123.

(38) Zhang, Q.; Jie, J.; Diao, S.; Shao, Z.; Zhang, Q.; Wang, L.; Deng, W.; Hu, W.; Xia, H.; Yuan, X.; Lee, S.-T., Solution-Processed Graphene Quantum Dot Deep-UV Photodetectors. *ACS Nano* **2015,** *9* (2), 1561-1570.

(39) Xu, X.; Xu, C.; Hu, J., High-Performance Deep Ultraviolet Photodetectors Based on ZnO Quantum Dot Assemblies. *J. Appl. Phys.* **2014,** *116* (10), 103105.

(40) Ghosh, D.; Kapri, S.; Bhattacharyya, S., Phenomenal Ultraviolet Photoresponsivity and Detectivity of Graphene Dots Immobilized on Zinc Oxide Nanorods. *ACS Appl. Mater. Interfaces* **2016,** *8* (51), 35496-35504.

(41) Li, L.; Gu, L.; Lou, Z.; Fan, Z.; Shen, G., ZnO Quantum Dot Decorated $Zn_2SnO_4$

Nanowire Heterojunction Photodetectors with Drastic Performance Enhancement and Flexible Ultraviolet Image Sensors. *ACS Nano* **2017,** *11* (4), 4067-4076.

**TOC graphic**

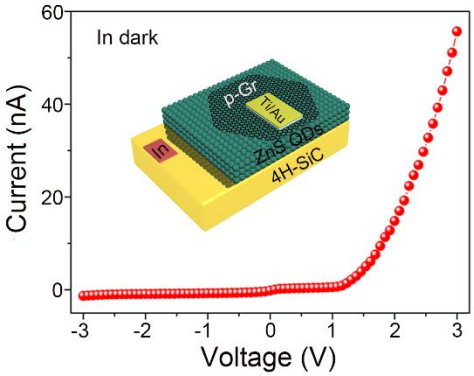
In dark
p-Gr
Ti/Au
In
ZnS QDs
4H-SiC
Current (nA)
Voltage (V)
60
40
20
0
-3
-2
-1
0
1
2
3